IN VIVO DEMONSTRATION OF ENHANCING GAS-FILLED MICROBUBBLE MAGNETIC SUSCEPTIBILITY WITH IRON OXIDE NANOPARTICLES

A. M. Chow[1,2], K. W. Chan[1,2], and E. X. Wu[1,2]

[1]Laboratory of Biomedical Imaging and Signal Processing, The University of Hong Kong, Pokfulam, Hong Kong SAR, China, People's Republic of,
[2]Department of Electrical and Electronic Engineering, The University of Hong Kong, Pokfulam, Hong Kong SAR, China, People's Republic of

INTRODUCTION

Gas-filled microbubbles have been recently employed in therapeutic applications due to their unique cavitation and sonoporation properties[1,2]. Local microbubble cavitation by spatially focused ultrasound can be applied in achieving site-specific release of incorporated drugs or genes inside microbubbles. Microbubbles can potentially be visualized by MRI and serve as an intravascular susceptibility contrast agent *in vivo* due to the induction of large local magnetic susceptibility difference by the gas-liquid interface[3-5]. However, microbubble susceptibility effect is relatively weak when compared with other intravascular MR susceptibility contrast agents. Previous theoretical and phantom studies have indicated that, by embedding or coating magnetic nanoparticles, the magnetic susceptibility of the shell can be increased[4,6,7], thus enhancing the microbubble susceptibility effect. In this study, we aim to further demonstrate the synergistic effect of gas core with iron oxide nanoparticles in achieving the overall microbubble susceptibility effect and characterize *in vivo* enhancements of microbubble susceptibility effects by entrapping iron oxide nanoparticles using dynamic susceptibility weighted MRI at 7 T.

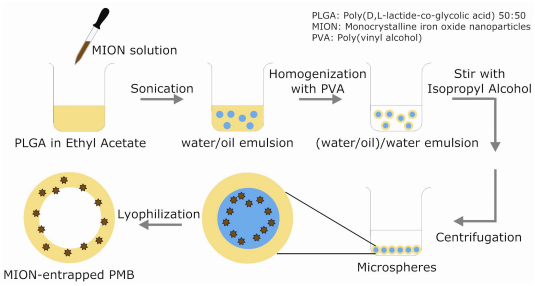

FIG. 1 Flow diagram representing the adapted double emulsion method for synthesizing iron oxide nanoparticles entrapped polymeric microbubbles (PMBs).

METHODS

All MRI experiments were performed on a 7 T Bruker MRI scanner. ***Synthesis of iron oxide nanoparticles entrapped polymeric microbubbles:*** Polymeric microbubbles (PMBs) with monocrystalline iron oxide nanoparticles (MIONs; MGH) incorporated or entrapped in shells were produced as previously described[6] (Fig. 1). To demonstrate the synergistic effect of the gas core with MIONs, MION-entrapped solid microspheres (without gas core) were also prepared with the same procedures without performing lyophilization for comparison. ***Characterization of PMBs:*** ΔR_2^* was measured by acquiring multi-echo GE signals continuously without phase encoding for 2 min as previously described[6]. The absolute iron contents were determined with inductively coupled plasma mass spectrometry (ICP-MS) for MION-entrapped PMBs and solid microspheres. Their r_2^* relaxivities were computed as the R_2^* in the initial uniform suspended state normalized with their respective iron contents. ***Animal Preparation and Microbubbles Administration:*** Normal SD rats (~250-350 g) ($N = 6$) were injected intravenously with 0.2 mL of microbubble suspension (~3.5% volume fraction) at a rate of 0.6 mL/min to avoid possible microbubble destruction due to high pressure and shear stress under femoral vein catheterization. The susceptibility effect of microbubbles was compared with SonoVue® (Bracco), by single dose of ~3.5% volume fraction injection using identical injection protocol and imaging sequence. ***MRI:*** Anatomical images were acquired using 2D FLASH sequence with resolution = $0.2 \times 0.2 \times 2$ mm^3. Dynamic susceptibility weighted liver MRI was performed with respiratory-gated single-shot GE-EPI sequence using TR ≈ 1000 ms, TE = 10 ms, FA = 90º, FOV = 50×50 mm, slice thickness = 2 mm, acquisition matrix = 64×64, BW = 221 kHz and NEX = 1. ***Image Analysis:*** GE-EPI images were first co-registered using AIR5.2.5[8]. ΔR_2^* maps were computed as previously described[9]. To quantify the ΔR_2^* values, ROIs were manually drawn in homogeneous liver region (LV) and the region covering blood vessel (BV) based on the high resolution FLASH images. Two-tail paired Student's t test was employed to compare the liver ΔR_2^* induced by MION-free and MION-entrapped PMBs with $p < 0.05$ considered as statistically significant. Assuming that ΔR_2^* is proportional to microbubble concentration C(t) at time t, C(t) were approximately modeled with a gamma-variate function by curve fitting given the relatively long injection time and the limited lifetime of microbubbles *in vivo*[5,9]. Full width at half maximum (FWHM) and time-to-peak were then measured from the fitted C(t) time courses.

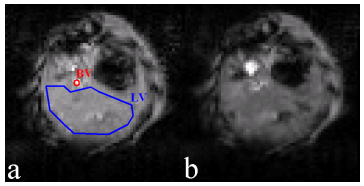

FIG. 2 GE-EPI T_2^*-weighted image for MION-entrapped PMB (0.2 mL of ~3.5% volume fraction) (a) preinjection image and (b) postinjection with the maximum susceptibility contrast.

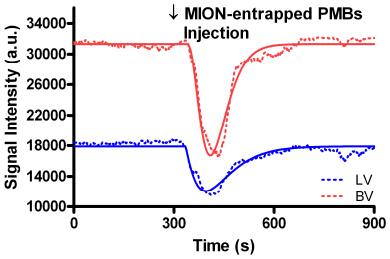

FIG. 3 T_2^*-weighted signal time courses in different liver regions during MION-entrapped PMB injection in the same rat. Two ROIs for time course measurement are shown in Fig. 1(a). Gamma-variate fitted data are shown in sold lines.

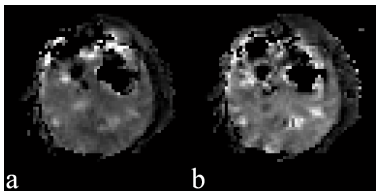

FIG. 4 ΔR_2^* maps for (a) MION-free and (b) MION-entrapped PMBs.

RESULTS AND DISCUSSIONS

Table 1 shows the measurements of the ΔR_2^* values and relaxivities for MION-entrapped PMBs ($N = 6$), MION-free PMBs ($N = 6$) and MION-entrapped microspheres ($N = 2$). ΔR_2^* for MION-entrapped PMBs was significantly higher than that of MION-free PMBs and MION-entrapped solid microspheres. The relaxivity results underscore the importance of both gas core and entrapped MIONs in achieving strong overall microbubble susceptibility effect, as suggested by the earlier theoretical study[7]. Figure 2(a) illustrates one of the preinjection GE-EPI T_2^*-weighted images, while (b) shows the corresponding postinjection GE-EPI T_2^*-weighted image with the maximum susceptibility contrast for MION-entrapped PMB injection. Figure 3 depicts the typical T_2^*-weighted signal time courses during PMBs injection with ROIs indicated in Fig. 2(a). Similar signal time course was also observed during MION-free PMB and SonoVue® injection. For MION-entrapped PMBs, the T_2^*-weighted signals after microbubble injection did not return to the preinjection baseline, this may be caused by accumulation of released MION in Kupffer cells after *in vivo* microbubble clearance. The computed ΔR_2^* maps for MION-free PMBs and MION-entrapped PMBs in the same animal were shown in Fig. 4, reflecting the blood distribution in tissue vasculature. Table 2 shows the *in vivo* measurements of the ΔR_2^*, FWHM and time-to-peak of MION-free PMBs, MION-entrapped PMBs and SonoVue® in liver among all rats studied. ΔR_2^* induced by MION-entrapped PMBs was found to be significantly higher than that by MION-free PMBs ($p < 0.05$), demonstrating that *in vivo* microbubble susceptibility can be enhanced by the MIONs entrapped in shells, as suggested by the earlier theoretical[7] and phantom studies[6].

Table 1 Measurements of ΔR_2^* values and relaxivities for MION-free PMBs ($N = 6$), MION-entrapped microspheres ($N = 2$), and MION-entrapped PMBs ($N = 6$) (mean ± standard error).

	ΔR_2^* (s^{-1})	Relaxivity (s^{-1}/(μg Fe mL^{-1}))
MION-free PMBs	79.2 ± 17.5	N.A.
MION-entrapped microspheres	82.5 ± 3.6	7.2
MION-entrapped PMBs	301.2 ± 16.8	21.0

Table 2 Measurements of ΔR_2^*, FWHM and time-to-peak of the concentration time courses for MION-free, MION-entrapped PMBs and SonoVue® in rat liver ($N = 6$) (mean ± SD).

	ΔR_2^* (s^{-1})	FWHM (s)	Time-to-peak (s)
MION-free PMBs	19.9 ± 14.5	81 ± 43	107 ± 31
MION-entrapped PMBs	28.9 ± 16.3	120 ± 76	100 ± 23
SonoVue®	9.4 ± 3.5	148 ± 59	141 ± 62

CONCLUSIONS

In this study, synergistic effect of gas core with iron oxide nanoparticles in achieving the overall microbubble susceptibility effect were shown, considerable susceptibility induced changes were observed and characterized in rat liver using MION-free and MION-entrapped PMBs, as well as SonoVue®. We demonstrated that entrapping iron oxide nanoparticles in polymeric microbubbles is feasible to significantly enhance magnetic susceptibility effects. With such approach, microbubbles can be monitored by MRI with higher sensitivity or lower concentrations, which may lead to the practical use of microbubbles as an intravascular MRI contrast agent, and MRI guidance in various microbubble-based drug delivery and therapeutic applications.

ACKNOWLEDGEMENTS This work was supported by GRF7642/06M.

REFERENCES [1] Ferrara KW. Adv Drug Deliv Rev 2008;60:1097-1102. [2] Unger EC, et al. Prog Cardiovasc Dis 2001;44:45-54. [3] Alexander AL, et al. Magn Reson Med 1996;35:801-806. [4] Dharmakumar R, et al. Magn Reson Med 2002;47:264-273. [5] Wong KK, et al. Magn Reson Med 2004;52:445-452. [6] Chow AM, et al. Magn Reson Med 2009;(in press). [7] Dharmakumar R, et al. Phys Med Biol 2005;50:4745-4762. [8] Woods RP, et al. J Comput Assist Tomogr 1998;22:139-152. [9] Cheung JS, et al. Neuroimage 2009;46:658-664.